Study of Isothermal Parameters for Adsorptive Uptake of Orange G dye: An Overview of Non-linear Approach and Error Analysis

Abstract

In this research, effort to convert waste to wealth was explicated in the usage of agro waste materials of regenerative resource, almond endocarp (*Terminalia catappa)* and tamarind seeds (*Dialium guineense*), as precursors for activated carbon production through thermal and chemical activation. The equilibrium adsorptive uptake of Orange G dye (OG) on almond endocarp salt activated (AESA) and tamarind seeds salt activated (TSSA) adsorbents was described using two-parameter (Langmuir and Freundlich) and three-parameter (Redlich-Peterson (R-P), Toth and Khan) isotherms employing the non-linear regression method. The best fit model in optimum isotherm prediction was investigated using four different error functions namely: root mean square error (RMSE), chi square (χ^2), mean absolute error (MAE) and coefficient of determination (R^2). Evaluation of the error estimation methods at 323K and 313K solution temperatures revealed that Khan and Toth; and Toth and Freundlich isotherms best described the experimental equilibrium data for AESA and TSSA sorption processes respectively. Examination of Langmuir's separation factor and Freundlich's surface heterogeneity factor suggest that the sorption process is favourable. Analysis of the calculated ANOVA F-values and probability values show that all the error functions under investigation were adequate in approximating the experimental data. The Coefficient of non-determination (K^2) values were useful in identifying the best error function in selecting the best isotherm. For the two-parameter isotherm at 323K solution temperature, RMSE function best minimized the error distribution between the experimental equilibrium data and theoretical isotherms while RMSE and R^2 functions were found to be the best for three-parameter isotherms studied.

Keywords: Adsorption. Orange G dye. Isotherm. Non-linear regression. Error functions

Introduction

The 21st century is posed with environmental pollution challenge emanating from untreated municipal and industrial effluents. According to Kumar *et al.* (2010), "industrial wastewater effluents from textiles, leather, rubber, paper and plastics contain several kinds of synthetic dye stuffs". "Dyes are essentially coloured organic compounds with very complex structures that can stain other substances" (Wang *et al.*,2018; Yagub *et al.*, 2014). It is reported that over 700,000 tons of different dyes are used in industrial production (Wang *et al.*,2018; Dawood and Sen, 2012) and more than 20% of effluent pollution comes from above dyes each year (Babalolac et al., 2016; Banerjee et al., 2017). Sequel to this, the availability of clean water supplies is becoming very much difficult owing to threats from industrial discharges (Yu *et al.,* 2016). "Dyes contaminate not only the environment but also traverse through the entire food chain leading to biomagnifications" (Bayramoglu *et al.*, 2009).

Substantial dyes are carcinogenic, mutagenic, stable to biological degradation (Ojedokun and Bello, 2017) "due to their complex aromatic structures, which provide them physicochemical, thermal and optical stability, thus bringing some difficulties for the treatment of these dyes"

(Kumar *et al.,* 2010). Orange G dye (OG) studied "in this research is reported to be highly toxic to human beings due to its carcinogenic and teratogenic nature". "OG is a monoazo, negatively charged dye and is widely used in printing and textile industries" (Banerjee *et al.,* 2019). A leading environmental challenge therefore, is to remove dyes from industrial and municipal effluents owing to its toxicity even at low concentration and distortion of the aesthetics of our environment.

"Diversified array of treatment technologies are being studied such as chemical oxidation, electro catalytic degradation, reverse osmosis, membrane filtration, coagulation/flocculation, adsorption, microbial degradation for the removal of dyes in the wastewater" (Wang *et al.,* 2018; Blanco *et al.,* 2017; Inyinbor *et al.,* 2016). "Adsorption is considered most promising and very effective separation technique, therefore preferred to other technologies for water treatment on account of its initial cost, simplicity of design, ease of operation and insensitive to toxic substance" (Li *et al.,* 2016; Dawood and Sen, 2012; Sen *et al.,* 2011; Mohammed *et al.,* 2010). This may be hinged on transfer of solute molecules onto an active adsorbent surface (Ghasemi *et al.,* 2014). Porous structures and functional groups which characterize the high uptake capacities of activated carbon present them as choice adsorbents for the treatment of pollutants. The increasing demand and high cost of activated carbon has necessitated the search of alternatives.

Researchers have demonstrated that utilization of inexpensive agro waste materials can efficiently solve the challenge of indiscriminate disposal of waste materials and also serve as precursor for preparation of materials for remediation of effluents from industrial and municipal origin. Some non-conventional and low cost adsorbents such as *Cedrela odorata* seed (Babalolac et al., 2016), cashew nut shells (Kumar *et al.,* 2010), *raphia hookeri* seeds (Okoye *et al.,* 2019), oil bean seed shells (Okey-Onyesolu *et al.,* 2018), sawdust (Ghasemi *et al.,* 2014) have been used for the removal of dyes in wastewater. In the current research, agro wastes: almond endocarp (*Terminalia catappa)* and tamarind seeds (*Dialium guineense*) of abundant regenerative resource were selected for investigation.

Literature search reveals that there is scanty or no publication to the best of our knowledge on the usage of NaCl activated almond endocarp (*Terminalia catappa)* and tamarind seeds (*Dialium guineense*) as an effective adsorbent for the removal of OG from aqueous solution. "Performance of an adsorption process is usually predicted from equilibrium sorption isotherms. Least square method is commonly used as a technique in searching for the best-fit sorption isotherm in predicting the optimum isotherm" (Kumar *et al.,* 2008). "The linear method is based on the assumption that the scatter vertical points around the line follows a Gaussian distribution, and the error distribution is uniform at every value of the x-axis" (Kumar, 2007). "This assumption is rarely true or practically impossible, as most of the adsorption isotherm models are nonlinear due to different mechanisms. Thus, the error distribution gets altered on transforming a nonlinear isotherm model to a linearized form" (Chowdhury, 2011).

In recent times, researchers have reported non-linear method as the best way to selecting the optimum isotherm (Allen *et al.,* 2003; Ho, 2004; Kumar and Sivanesan, 2007; Shahmohammadi-Kalalagh, and Babazadeh, 2014). Non-linear regression method was therefore adopted for this

study. This method involves a step of minimizing the error distribution between the experimental data and predicted isotherm using error functions. This present research compared the performance of four error functions in approximating the error distribution between the experimental and five predicted isotherms for OG adsorptive uptake onto AESA and TSSA. The Langmuir, Freundlich, Redlich-Peterson, Toth and Khan isotherms were considered for the study.

2. Materials and Methods

2.1 Materials

Agricultural waste materials, Almond endocarp (*Terminalia catappa*) and Tamarind seeds (*Dialium guineense*) used for adsorbent preparation were obtained from St Mark's Nibo-Nise in Anambra state and Amasiri in Ebonyi state respectively. Orange G dye (OG) and other chemicals of analytical grades were purchased from a chemical vendor at Head Bridge Onitsha, Anambra State, Nigeria and used without further purification.

2.2 Methods

2.2.1 Adsorbent preparation

Tamarind seeds and Almond endocarp were properly washed with distilled water to remove unwanted contaminants, air-dried for 6 hours and further oven dried for 4 hours at a temperature of 383K to ensure constant weight. The almond endocarp was further reduced to smaller particle sizes. The activated carbon production procedure reported by Okoye *et al.,* (2019) was adopted with necessary modification to suit the precursors. Tamarind seeds and almond endocarp were left for one hour at 873K and one and half hours at 873K in a muffle furnace respectively. 60% by weight sodium chloride salt (NaCl) solution was used as the activating agent. Impregnation ratio is defined as the ratio of amount of chemical used for activation (in g) to the amount of precursor (biomass sample) (in g) used. The thermally activated samples were impregnated at ratio 1:1 and 1:2 weight basis of activating agent to tamarind seeds and almond endocarp respectively. The slurry was vigorously stirred and allowed for 24 hours. The resulting carbon was rinsed with distilled water until the pH of the leachate was between 6 and 8. They were then dried in an oven at temperature of 105^0C for 5-6 hours. The oven dried activated carbon was reduced in size with mortar and pistil and sieved using 75µm mesh size. The activated carbons produced were stored in properly labelled air tight containers for further experiments.

2.2.2 Adsorbent characterization

The functional groups present in AESA and TSSA were determined using FTIR spectrophotometer (Shimadzu FTIR 8400) over a range of 4000 – 400 cm^{-1}.

2.2.3 Batch adsorption studies

The adsorptive performance of AESA and TSSA were determined by batch experiments at 75 µm adsorbent particle size, 1 g adsorbent dosage and pH 2 obtained in preliminary experiments, adopted from Okoye (2014) at varying temperatures and concentrations.

The steps for the sorption experiment are described below:

1. Series of 250 ml Pyrex beakers containing 100 ml of 100 mg/L concentration of OG and specified dosage of AESA and TSSA were set at 303K, 313K and 323K respectively.

2. The contents of the beakers were agitated using a magnetic stirrer at speed of 110 rev/min. Aliquots were withdrawn from the beakers and filtered using Whatman No. 1 filter paper at the end of the predetermined time.
3. The amount of unadsorbed dye in each supernatant solution was tested using a visible spectrophotometer. The procedure is repeated at set temperatures and varying concentrations (100, 150, 200 and 300mg/L). The sorption capacity (mg/g) was calculated by the relationship:

$$q_e = \frac{(C_o - C_e)V}{m} \quad (1)$$

where qe is the amount of dye adsorbed (mg/g), m is the weight of adsorbent (g), V, volume of the dye solution and Co and Ce, the dye concentration (mg/L) at the initial time and at a time t, respectively.

2.3 Theory

2.3.1 Adsorption isotherm

"Adsorption isotherm describes the relationship between the amount of adsorbate adsorbed and the adsorbent; the concentration of dissolved adsorbate in the liquid equilibrium" (Rameshraja *et al.,* 2012). "To explicate adsorbent-adsorbate interaction, Langmuir, Freundlich, Redlich-Peterson, Toth and Khan models were chosen to simulate the adsorption isotherm. Table 1 presents the non-linear equations of the selected models. Langmuir isotherm model assumes that adsorption is limited to a monolayer, adsorbent surface is homogeneous, adsorption energy is uniform for all sites and there is no transmigration of adsorbate in the plane of the surface" (Saadi *et al.,* 2015). The essential characteristics of the Langmuir equation can be expressed in terms of a dimensionless separation factor R_L (equation 3). "The Freundlich isotherm model is used for heterogeneous surface energy systems and for description of multilayer adsorption with interaction between adsorbed molecules" (Piccin *et al.,* 2011). The values of Freundlich's surface heterogeneity factor (1/ n) between 0 and 1 indicates favorable adsorption isotherm (Saadi *et al.,* 2015). The constant, K_f, is an approximate indicator of adsorption capacity (Voudrias and Bozani, 2002). The Redlich-Peterson (R-P) isotherm model includes the characteristics of Langmuir and the Freundlich isotherms (Saadi *et al.,* 2015) and can be applied in either homogeneous or heterogeneous systems due to its versatility (Piccin *et al.,* 2011). "Toth isotherm model is an empirical modified form of the Langmuir equation. Mostly, this isotherm model is utilized for the description of heterogeneous adsorption system; satisfying the low and high concentration of adsorbate" (Al-Ghouti and Da'ana, 2020). This model assumes a quasi-Gaussian energy distribution, where most sites have adsorption energies lower than the peak or maximum adsorption energy (Padmesh *et al.,* 2006). "The Khan isotherm model covers both extremes, Langmuir and Freundlich descriptions. It is a generalized model developed for both multicomponent and single component adsorption systems and suggested for pure solutions" (Saadi *et al.,* 2015).

Table 1: Adsorption isotherm models

Isotherm models	Non-linear equation	Equation no	Reference
Langmuir	$q_e = \frac{q_m k_L C_e}{1 + k_L C_e}$	2	
	$R_L = \frac{1}{1 + k_L C_o}$	3	Bayramoglu *et al.*, 2009
Freundlich	$q_e = k_f C_e^{1/n}$	4	Padmesh *et al.*, 2006
Redlich-Peterson	$q_e = \frac{k_{RP} C_e}{1 + a_{RP} C_e^g}$	5	(Al-Ghouti and Da'ana, 2020)
Toth	$q_e = \frac{q_{mT} b_T C_e}{[1 + (b_T C_e)^{1/n_T}]^{n_T}}$	6	Padmesh *et al.*, 2006
Khan	$q_e = \frac{q_{mk} b_k C_e}{1 + (b_k C_e)^{a_k}}$	7	(Al-Ghouti and Da'ana, 2020)

3. Results and Discussion

3.1 Instrumental characterization

3.1.1 FTIR

Figures A and B show plots of %Transmittance against wave number for AESA and TSSA. Functional groups were assigned to distinct peaks of AESA spectrum, 635.57cm^{-1} show the presence of alkyne C-H bend, 856.42 cm^{-1}and 1151.54 cm^{-1} were assigned to C-H aromatics and C-H in-plane bend respectively, 1637.62 cm^{-1}, 1794.82 cm^{-1} and 2279.94 cm^{-1} depict the presence of alkenyl C=C stretch, -C=O stretching and $-C \equiv N$ stretch, nitriles respectively. Other bands detected can be assigned to C–H stretching (2931.90 cm^{-1}), Hydroxy group, H-bonded O-H stretch (3405.44 cm^{-1}) and O-H stretch in phenols and alcohols(3823.04 cm^{-1}). The notable peaks for TSSA were registered at 649.07cm^{-1} (alkyne C-H bend), 734.90 cm^{-1} (C-Cl stretch), 1154.43 cm^{-1} (C-H in-plane bend), 1266.31 cm^{-1} (aromatic primary amine), 1646.30 cm^{-1} (alkenyl C=C stretch), 2252.93 cm^{-1} ($-C \equiv C$ stretch), 2429.42-2665.71 cm^{-1} (O-H stretch, carboxylic acid), 3450.77 cm^{-1} and 3553.96 cm^{-1} (Hydroxy group, H-bonded O-H stretch), 3796.04 cm^{-1} (O-H stretch in phenols and alcohols). The adsorbent containing these bends are usually utilized for colour removal (Patel and Vashi, 2010).

3.2 Influence of concentration and temperature

Figure 1 and 2 describe the adsorption of OG on AESA and TSSA respectively examined at various initial OG concentration (100, 150, 200 and 300mg/l) at 303, 313 and 333K solution temperature. The results reveal that there exist a relationship between the adsorbate concentration and available active sites on the adsorbents' surface at all the temperatures studied. The trend followed by the plots shows a direct proportional relationship between the amount of

dye adsorbed per gram of adsorbent (q_e) and the initial concentration (C_o). The observed trend is possibly because the initial dyes concentration provides an important driving force to overcome all mass transfer resistances of the dye molecules between the aqueous and solid phases. Hence, a higher initial concentration of dye will enhance the adsorption process (Bayramoglu *et al.*, 2009). The increased amount of OG adsorbed per gram of adsorbent (q_e) observed at temperatures above ambient condition may be due to the fact that higher temperatures accelerate the rate of diffusion of the dye molecules from the surface to the internal pores of the adsorbent, also, temperature changes alter equilibrium between the adsorbent and the adsorbate (Schimmel *et al.*, 2010).

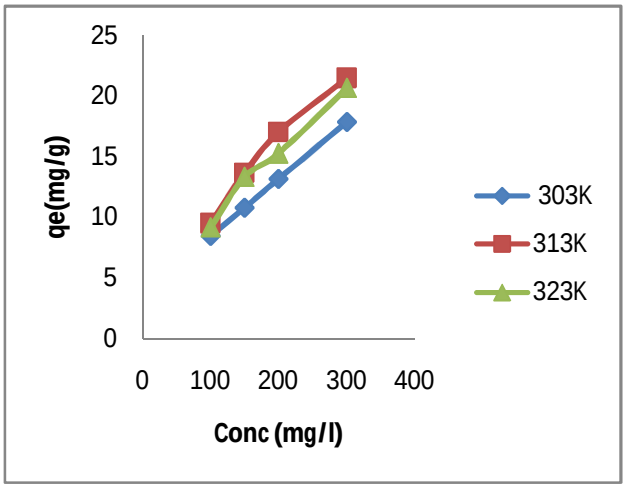

Figure 1: Effect of Concentration on amount of OG adsorbed on AESA

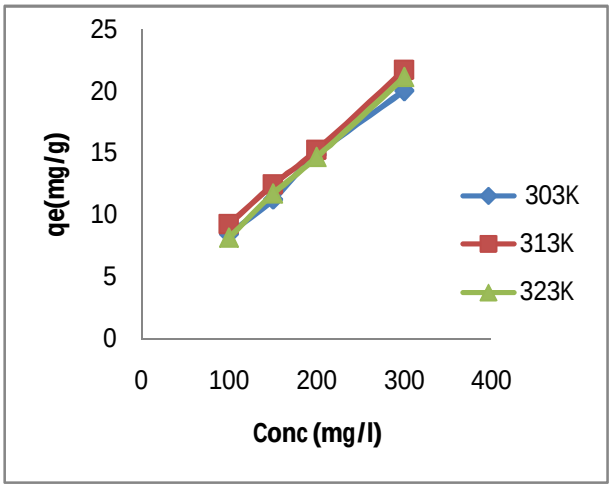

Figure 2: Effect of Concentration on amount of OG adsorbed on TSSA

3.3 Adsorption Isotherm study

Findings from previous research reports reveal innate bias emanating from conventional model linearization of non-linear experimental data. Sometimes, this may lead to violation of the theories behind the isotherm. Sequel to these inefficiencies, non-linear regression method was used to evaluate the isotherm behaviour of the adsorptive process using two-parameter (Langmuir and Freundlich) and three-parameter (Redlich-Peterson, Toth and Khan) isotherm models. Predicted isotherm using the non-linear method vary with the error function used while minimizing error difference between experimental and predicted isotherms (Shahmohammadi-Kalalagh, and Babazadeh, 2014; Kumara *et al.*, 2008; Wong *et al.*, 2004; Allen *et al.*, 2003). Therefore, four error functions: root mean square error (RMSE), chi-square (χ^2), mean absolute error (MAE) and coefficient of determination (R^2) were employed to investigate the influence of error functions on predicted isotherms. The descriptions of the error functions are presented in Table 2.The isotherm parameters were computed by minimizing or maximizing the error function using the solver add-in function in Microsoft Excel.

Table 2: Error functions and its equations

Error function	Equation and number	Reference
Root mean square error	$\mathrm{RMSE} = \sqrt{\frac{1}{n}\sum_{i=1}^{n}\left(y_{i,exp} - y_{i,pred}\right)^2}$ (8)	Pakravan *et al.*, 2014
Chi square (χ^2)	$\chi^2 = \sum_{i=1}^{n} \frac{\left(y_{i,p} - y_{i,e}\right)^2}{y_{i,p}}$ (9)	Padmesh *et al.*, 2006
Mean absolute error	$MAE = \frac{1}{n}\sum_{i=1}^{n}\left\|\left(y_{i,exp} - y_{i,pred}\right)\right\|$ (10)	Betiku *et al.*, 2016
Coefficient of determination	$R^2 = \left(\frac{n\left(\sum y_{i,exp} \cdot y_{i,pred}\right) - \left(\sum y_{i,exp}\right)\left(\sum y_{i,pred}\right)}{\sqrt{\left[n\sum y_{i,exp}{}^2 - \left(\sum y_{i,exp}\right)^2\right]\left[n\sum y_{i,pred}{}^2 - \left(y_{i,pred}\right)^2\right]}}\right)^2$ (11)	Tuttuh-Adegun, M. R. and Adegoke, D. G. (2013)

At 323K, Figures 3(a-e) and 4(a-e) depict plots of the experimental and predicted Langmuir, Freundlich, Redlich-Peterson, Toth and Khan isotherms respectively for adsorptive uptake of OG on AESA and TSSA obtained by using the error functions to approximate the error distribution between the experimental equilibrium data and the predicted isotherms. It was observed that the error functions had varying effects on the predictability of all the investigated two-parameter and three-parameter isotherm models for AESA and TSSA adsorption processes (Figures 3a-e and 4a-c,e) except for Toth three-parameter (Figure 4d). Similar trend was also observed at solution temperature 313K (Figures C (a,b) and D (a-e)). However, Figures C (c, d & e) show that the predicted Redlich-Peterson, Toth and Khan isotherms remained almost the same, regardless of the error function used for OG adsorption on AESA.

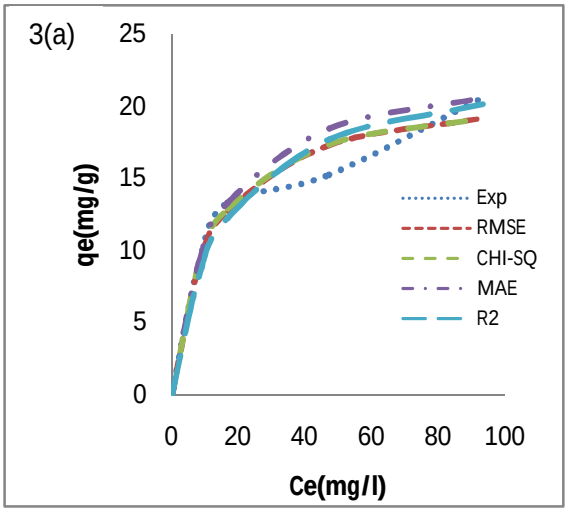
3(a)
25
20
15
10
5
0
qe(mg/g)
0
20
40
60
80
100
Ce(mg/l)
Exp
RMSE
CHI-SQ
MAE
R2

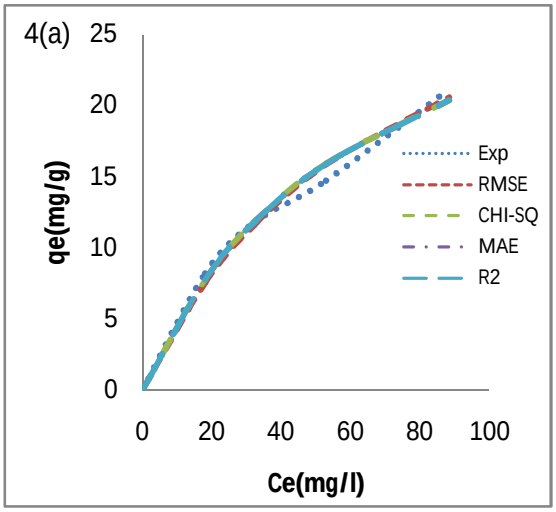
4(a)
25
20
15
10
5
0
qe(mg/g)
0
20
40
60
80
100
Ce(mg/l)
Exp
RMSE
CHI-SQ
MAE
R2

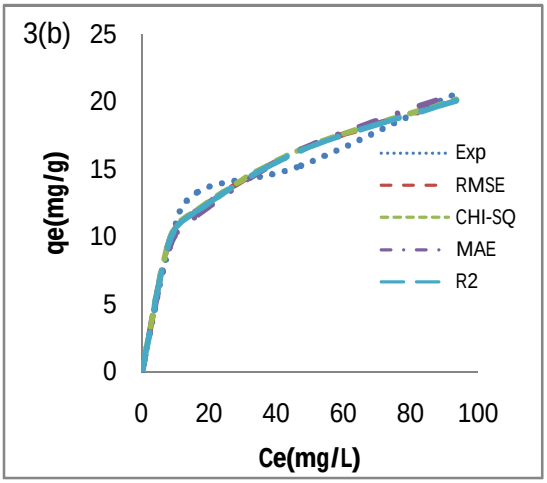
3(b)
25
20
15
10
5
0
qe(mg/g)
0
20
40
60
80
100
Ce(mg/L)
Exp
RMSE
CHI-SQ
MAE
R2

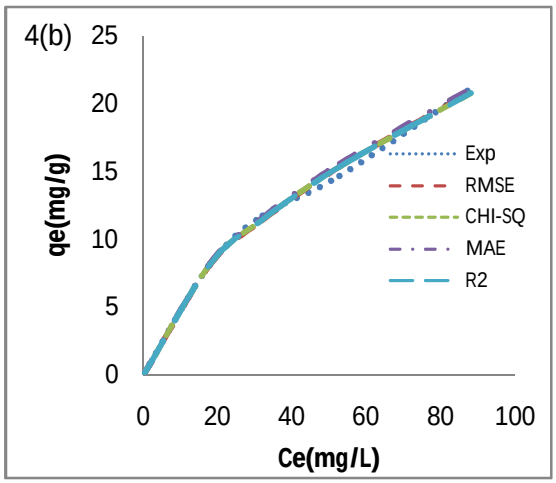
4(b)
25
20
15
10
5
0
qe(mg/g)
0
20
40
60
80
100
Ce(mg/L)
Exp
RMSE
CHI-SQ
MAE
R2

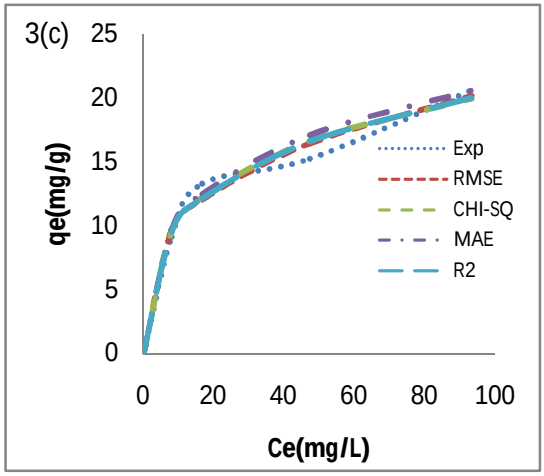
3(c)
25
20
15
10
5
0
qe(mg/g)
0
20
40
60
80
100
Ce(mg/L)
Exp
RMSE
CHI-SQ
MAE
R2

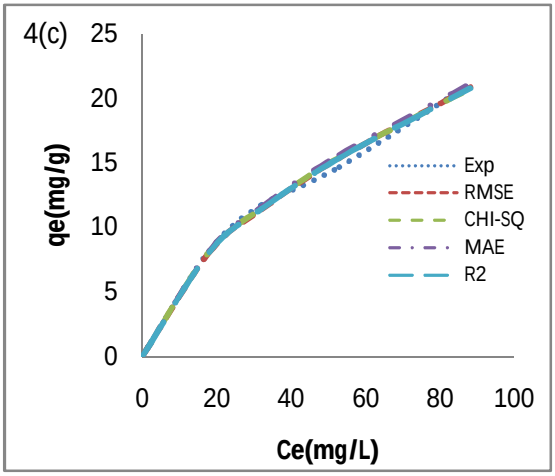
4(c)
25
20
15
10
5
0
qe(mg/g)
0
20
40
60
80
100
Ce(mg/L)
Exp
RMSE
CHI-SQ
MAE
R2

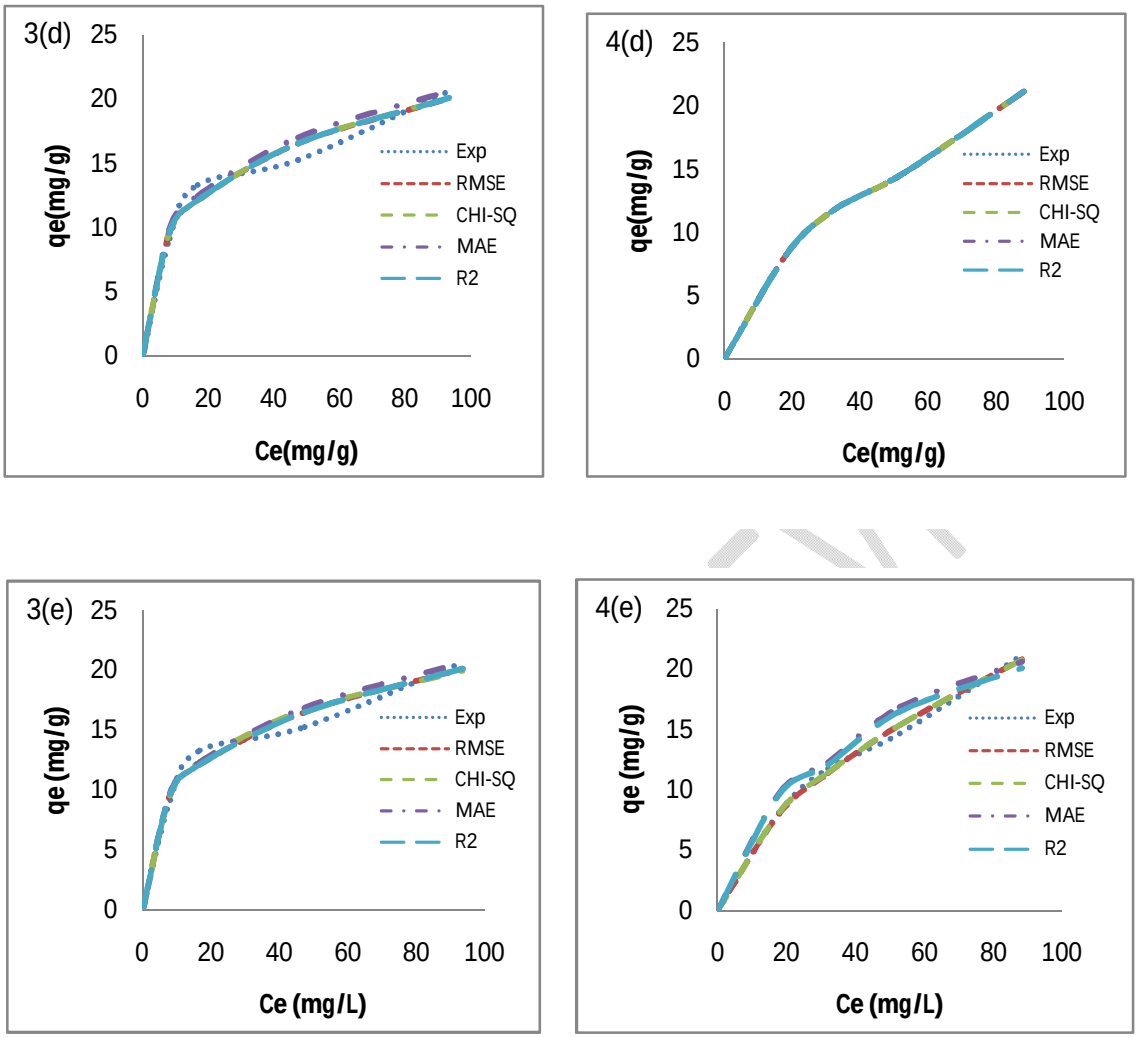

Figures 3 and 4: Fits of isotherm models by minimizing/maximizing error functions for OG onto AESA and TSSA respectively at 323K. (a) Langmuir (b) Freundlich (c) R-P (d) Toth (e) Khan

It was necessary subjecting the predicted data to further statistical test considering the fact that the nonlinear isotherm models fittings were conducted using an iterative process based on rational initial parameter guess which could introduce bias in the error functions. Therefore, ANOVA using MS Excel data analysis tool box was employed to evaluate the observed effect of error functions on the experimental equilibrium data. Table 3 presents relevant parameters used to examine if there is a statistical difference in the mean distances between the experimental and predicted isotherms obtained by minimizing/maximizing the respective error functions across the models. ANOVA infers whether three or more population means are equal. Analysis of F-values on Table 3 is in reference to their corresponding F-critical values. If F-value < F-critical, the null hypothesis (H_o) which states that the means of the population are equal is accepted ($Ho = \mu_1 = \mu_2 = \mu_3 = \ldots = \mu_k$; μ = mean) and alternate hypothesis (at least one of the means is different) is rejected. From Table 3, it could be seen that the F-values for both AESA ($F < 0.006597$) and

TSSA (F < 0.000441) at solution temperature of 323K were below the F-critical (2.86608). The null hypothesis is also accepted if p-value > confidence level. All significance tests provide results within a predefined confidence level of 5% (0.05). The p-values (Table 3) recorded both for AESA and TSSA were all above 0.05, therefore the null hypothesis is accepted. The results of these analyses suggest that all the investigated error functions were effective in minimizing the error distribution between the experimental and theoretical isotherms. This is in agreement with the observation also recorded at 313K (Table A).

Table 3: ANOVA table for AESA and TSSA

	Langmuir	Freundlich	R-P	Toth	Khan
AESA					
P-value	0.999991	1	0.999994	0.999993	0.999998
F-value	0.006597	0.000184	0.001654	0.001823	0.000979
F-critical	2.866081	2.866081	2.866081	2.866081	2.866081
TSSA					
P-value	1	1	1	1	1
F-value	4.97E-05	0.000441	0.000393	3.53E-13	8.04E-06
F-critical	2.866081	2.866081	2.866081	2.866081	2.866081

Tables 4 and 5 present calculated isotherm parameters and their corresponding objective functions for the minimum error distribution between the experimental and predicted isotherms for adsorption of OG on AESA and TSSA at 323K solution temperature respectively. Khan isotherm model with least error deviation values presented in Table 4 for RMSE, R^2 and χ^2 error functions coincides better with the experimental curve than the other models investigated. This reveals that the isotherm equilibrium data for OG uptake on AESA adsorbent best fitted Khan model. Table 5 shows that the coefficient of determination (R^2) value obtained for Toth isotherm is closest to unity compared to other four isotherms, suggesting that Toth isotherm best-fit the experimental data for OG adsorption on TSSA. A similar result can be deduced from the values of the other error functions: RMSE, χ^2 and MAE.

Toth model best described the equilibrium data for OG adsorption on AESA adsorbent at 313K solution temperature (Table B). It was however implausible to clearly consider R^2 as an adjuring yardstick for determination of the performance of the three-parameter models owing to the seeming confusion and fitting ambiguity orchestrated by the almost equivalent value (Redlich-Peterson (0.99997), Toth (0.99998) and Khan (0.99992) recorded for AESA adsorption. Table C depicts that adsorption of OG dye on TSSA equilibrium data best followed the Freundlich isotherm model. Freundlich's calculated parameter, 1/n, is the intensity of the adsorption or surface heterogeneity indicating the energy relative distribution and the adsorbate sites' heterogeneity. When $1/n$ is greater than zero ($0<1/n<1$) the adsorption is favorable, when $1/n$ is greater than 1, the adsorption process is unfavorable, and it is irreversible when $1/n = 1$ (Al-Ghouti and Da'ana, 2020). Table 5 shows that the calculated 1/n values were within the range of 0 and 1 thereby expressing that the adsorption process of OG uptake on TSSA is favourable. The best fit recorded by Freundlich isotherm shows that the adsorption proceeded at sites with varying energy of adsorption sites and heterogeneity of the adsorbent surface. Examination of all the Freundlich's intensity of adsorption parameter (1/n) calculated for OG adsorption on AESA

and TSSA at 313K and 323K show favourability of the adsorption process. The Langmuir's separation factor (R_L) calculated data were found to fall within a range of 0 – 1 (data not shown). This also buttresses the favourability of the adsorption processes as earlier suggested from Freundlich's intensity of adsorption parameter (1/n).

Table 4: Predicted isotherm by minimizing the error distribution using four different error function for AESA at 323K

Langmuir (two parameter isotherm)				
TSSA	q_m	K_L		OF[a]
R^2	23.4626	0.0658		0.9085
RMSE	21.6199	0.0863		1.1632
Chi-Square	21.5098	0.0896		0.3838
MAE	23.4625	0.0785		1.0783
Freundlich (two parameter isotherm)				
	n	K_f		OF[a]
R^2	3.3252	5.1399		0.9479
RMSE	3.3427	5.1910		0.8420
Chi-Square	3.3628	5.2367		0.2605
MAE	3.0110	4.5753		0.9579
Redlich-Peterson (three parameter isotherm)				
	K_{rp}	a_{rp}	g	OF[a]
R^2	7.99999	1.2057	0.7503	0.9467
RMSE	51.9970	9.6663	0.7080	0.8419
Chi-Square	6.2909	0.8679	0.7688	0.2480
MAE	6.2911	0.8666	0.7617	1.0723
Toth (three parameter isotherm)				
	q_{mT}	b_T	n_T	OF[a]
R^2	497.4896	157.1203	9.9425	0.9461
RMSE	497.4910	157.1187	9.9429	0.8564
Chi-Square	497.4896	157.1203	9.9387	0.2587
MAE	497.4898	157.1204	9.8958	1.1225
Khan (three parameter isotherm)				
	q_{mk}	b_k	a_k	OF[a]
R^2	4.5550	1.9866	0.7148	0.9482
RMSE	4.5551	1.9867	0.7148	0.8399
Chi-Square	8.0909	0.4927	0.7597	0.2429
MAE	4.5553	1.9868	0.7100	1.0783

Table 5: Predicted isotherm by minimizing the error distribution using four different error function for TSSA

Langmuir (two parameter isotherm)				
TSSA	q_m	K_L		OF[a]
R^2	35.0225	0.0158		0.9746
RMSE	37.3851	0.0140		0.6554
Chi-Square	35.0225	0.0158		0.1487
MAE	35.0225	0.0158		0.8179
Freundlich (two parameter isotherm)				
	n	K_f		OF[a]
R^2	1.6945	1.4801		0.9925
RMSE	1.6738	1.4375		0.3647
Chi-Square	1.6972	1.4861		0.0440
MAE	1.6859	1.4843		0.3713
Redlich-Peterson (three parameter isotherm)				
	K_{rp}	a_{rp}	g	OF[a]
R^2	4.5190	2.5403	0.4389	0.9921
RMSE	105.8585	73.0945	0.4037	0.3652
Chi-Square	4.5354	2.5186	0.4417	0.0467
MAE	4.5192	2.5399	0.4351	0.3614
Toth (three parameter isotherm)				
	q_{mT}	b_T	n_T	OF[a]
R^2	320.3138	0.0066	3.5558	1.0000
RMSE	320.3138	0.0066	3.5558	0.0000
Chi-Square	320.3138	0.0066	3.5558	1.00697E-11
MAE	320.3138	0.0066	3.5558	7.757E-06
Khan (three parameter isotherm)				
	q_{mk}	b_k	a_k	OF[a]
R^2	1.7557	0.7873	0.4146	0.9923
RMSE	1.7556	0.7872	0.4149	0.3753
Chi-Square	0.1348	58.8171	0.4109	0.0441
MAE	1.7556	0.7872	0.4149	0.4901

In order to investigate which error function best minimizes the error distribution between the experimental and theoretical isotherms, another statistical term, coefficient of non-determination, K^2, was employed (Shahmohammadi-Kalalagh and Babazadeh, 2014). The coefficient of non-determination, K^2, can be expressed as:

$$K^2 = \frac{Unexplained\ variance}{Total\ variance} = 1 - \frac{Explained\ variance}{Total\ variance} = 1 - r^2 \quad (12)$$

The coefficient of non-determination is a veritable tool in measuring the linear or non-linear co-variation of two variables. K^2 will help to a great extent in revealing the level of relationship between the experimental and isotherm predicted data. Calculated K^2 values for the investigated

isotherms predicted by minimizing/maximizing the various error functions at 313K and 323K were plotted on Figures 5a,b and Fig E (a,b). Considering the coefficient of non-determination results for the adsorption of OG on AESA and TSSA at 323K, RMSE function as observed in Figures 5a and b marginally outperformed R^2 and MAE in explaining the two-parameter isotherms (Langmuir and Freundlich), thus suggesting RMSE as seemingly the best in predicting the optimum isotherm if the aim is to choose the best-fit from the two parameter isotherms. For the investigated three-parameter isotherms, the top two approximations of the error distribution for the studied isotherm models were achieved employing RMSE and R^2. At 313K solution temperature while MAE and RMSE were observed as the best functions to least un-explain the two-parameter isotherms, RMSE function performed best for the three-parameter investigated isotherm models (Figures E (a and b)).

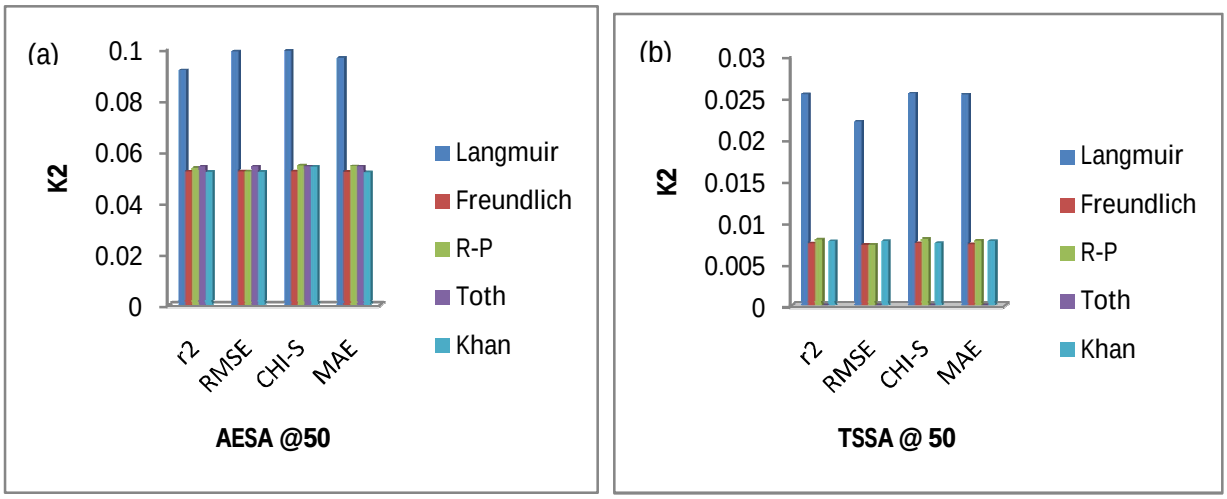

Figure 5: Coefficient of non-determination for isotherms of OG adsorbed on (a) AESA and (b) TSSA

4.0 Conclusion

Langmuir, Freundlich, Redlich-Peterson, Toth and Khan isotherms were used to explain the equilibrium sorption of OG onto AESA and TSSA adsorbents. Findings from comparison based on statistical evaluation show that the four error functions used to predict the two-parameter and three-parameter isotherm parameters and also predict the optimum isotherm were all adequate. Isotherm parameters calculated show that the adsorption process is feasible. The closest to unity R^2 and least RMSE, MAE and χ^2 showed that Khan and Toth isotherms best fitted the equilibrium experimental data for AESA and TSSA respectively at 323K while the equilibrium data best followed Toth and Freundlich at 313K solution temperature for AESA and TSSA respectively. Coefficient of non-determination was employed in comparing the efficiency error functions under investigation. RMSE and; RMSE and R^2 functions were found to be the best in minimizing error distribution between experimental data and predicted isotherms for two-parameter and three-parameter isotherms respectively at 323K solution temperature.

5.0 References

Al-Ghouti, M. A., Da'ana, D. A. (2020). Guidelines for the use and interpretation of adsorption isotherm models: A review, *Journal of Hazardous Materials*, doi: https://doi.org/10.1016/j.jhazmat.2020.122383

Allen SJ, Gan Q, Matthews R, Johnson PA (2003) Comparison of optimized isotherm models for basic dye adsorption by kudzu. Bioresour Technol 88(2),143–152.

Babalolac, J.O., Koikic, B.A., Eniayewuc, Y., Salimonuc, A., Olowoyoc, J.O., Oninlac, V.O., Alabic, H.A., Ofomajaa, A.E. and Omorogie, M.O. (2016). Adsorption efficacy of Cedrela odorata seed waste for dyes: non linear fractal kinetics and non linear equilibrium studies. J. Environ. Chem. Eng. 4,, 3527-3536.

Banerjee, P., Barman, S.R., Mukhopadhayay, A. and Das, P. (2017). Ultrasound assisted mixed azo dye adsorption by chitosan-graphene oxide nanocomposite. Chem. Eng. Res. Des., 117, 43-56.

Banerjee, S., Dubey, S., Gautam, R. K., Chattopadhyaya, M. C. and Sharma, Y. C. (2019). Adsorption characteristics of alumina nanoparticles for the removal of hazardous dye, Orange G from aqueous solutions. Arabian Journal of Chemistry, 12, 5339–5354

Bayramoglu, G., Altintas, B. and Arica, M. (2009). Adsorption kinetics and thermodynamic parameters of cationic dyes from aqueous solutions by using a new strong cation-exchange resin. Chemical Engineering Journal. 152, 339-346.

Betiku, E., Odude, V. O., Ishola, N. B., Bamimore, A., Osunleke, A. S. and Okeleye, A. A. Predictive capability evaluation of RSM, ANFIS and ANN: A case of reduction of high free fatty acid palm kernel oil via esterification process. Energy conversion and management. 2016: 124, 219-230.

Blanco, S.P.D.M., Scheufele, F.B., M_odenes, A.N., Quiñones, F.R.E., Marin, P., Kroumov, A.D. and Borba, C.E. (2017). Kinetic, equilibrium and thermodynamic phenomenological modeling of reactive dye adsorption onto polymeric adsorbent. Chem. Eng. J., 307, 466-475.

Chowdhury, S., Misra, R., Kushwaha, P. and Das, P. (2011). Optimum sorption isotherm by linear and nonlinear methods for safranin onto alkali-treated rice husk. Bioremediation Journal. 15(2), 77-89.

Dawood, S. and Sen, T. K. (2012). Removal of anionic dye Congo red from aqueous solution by raw pine and acid-treated pine cone powder as adsorbent: Equilibrium, thermodynamic, kinetics, mechanism and process design. Water research, 46, 1933-1946

Ghasemi, M., Naushad , Mu., Ghasemi, N., Khosravi-fard, Y. (2014). A novel agricultural waste based adsorbent for the removal of Pb(II) from aqueous solution: Kinetics, equilibrium and thermodynamic studies. Journal of Industrial and Engineering Chemistry, 20, 454–461.

Inyinbor, A. A., Adekola, F. A. and Olatunji, G. A. (2016). Kinetics, isotherms and thermodynamic modeling of liquid phase adsorption of Rhodamine B dye onto Raphia hookerie fruit epicarp. Water Resour. India, 15, 14-27.

Kumar, K. V. and Sivanesan, S. (2007) Sorption isotherm for safranin onto rice husk: comparison of linear and non-linear methods. Dyes Pigments. 72(1), 130–133.

Kumar, K. V. (2007). Optimum sorption isotherm by linear and non-linear methods for malachite green onto lemon peel. Dyes Pigments. 74, 595–597

Kumar, P. S., Ramalingam, S., Senthamarai, C., Niranjanaa, M., Vijayalakshmi, P. and Sivanesan, S. (2010). Adsorption of dye from aqueous solution by cashew nut shell: Studies on equilibrium isotherm, kinetics and thermodynamics of interactions. Desalination, 261, 52–60.

Kumar,V. K., Porkodi, K. and Rocha, F. (2008). Comparison of various error functions in predicting the optimum isotherm by linear and non-linear regression analysis for the sorption of basic red 9 by activated carbon. Journal of Hazardous Materials, 150, 158–165.

Li, S.B., Jia, Z.G., Li, Z.Y., Li, Y.H. and Zhu, R.S. (2016). Synthesis and characterization of mesoporous carbon nanofibers and its adsorption for dye in wastewater. Adv. Powder Technol. 27, 591-598.

Mohammad, M., Maitra, S., Ahmad, N., Bustam, A., Sen, T.K. and Dutta, B.K. (2010). Metal ion removal from aqueous solution using physic seed hull. J. Hazard. Mater. 179, 363-372.

Ojedokun, A. T. and Bello, O. S. (2017). Kinetic modeling of liquid-phase adsorption of Congo red dye using guava leaf-based activated carbon. Appl Water Sci.,7, 1965–1977.

Okey-Onyesolu, C.F., Okoye, C.C., Chime, D.C. (2018). Removal of Eosin yellow dye from aqueous solution using oil bean seed shells based activated carbons: Equilibrium, Kinetics and thermodynamics studies. International Journal of Scientific & Engineering Research, 9(3), 140-167.

Okoye, C. C. (2014). Removal of dyes from simulated wastewater using activated carbon from agro wastes. Nnamdi Azikiwe University, Awka, Nigeria, Unpublished M.Eng Thesis.

Okoye, C.C., Onukwuli, O.D. and Okey-Onyesolu, C.F. (2019). Utilization of salt activated Raphia hookeri seeds as biosorbent for Erythrosine B dye removal: Kinetics and thermodynamics studies. Journal of King Saud University – Science, 31, 849-858.

Padmesh, T. V. N., Vijayaraghavan, K., Sekaran, G. and Velan, M. (2006). Application of two- and three-parameter isotherm models: Biosorption of acid red 88 onto azolla microphylla. Bioremediation Journal, 10:1-2, 37-44, DOI:10.1080/10889860600842746

Pakravan, P., Akhbari, A., Moradi, H., Azandaryani, A. H., Mansouri, A. M. and Safari, M. Process modeling and evaluation of petroleum refinery wastewater treatment through response surface methodology and artificial neural network in a photocatalytic reactor using polyethyleneimine (PEI)/titania (TiO2) multilayer film on quartz tube. Appl Petrochem Res. 2014: 5,47–59.

Patel, H. and Vashi, R. T. (2010). Adsorption of crystal violet dye onto Tamarind seed powder. Journal of Chemistry. 7(3), 975-984.

Piccin, J. S., Dotto, G. L. and Pinto, L. A. A. (2011). Adsorption isotherms and thermochemical data of FD&C red N°40 binding by chitosan. Brazilian Journal of Chemical Engineering, 28(2), 295 – 304.

Saadi, R., Saadi, Z., Fazaeli, R. and Fard, N. E. (2015). Monolayer and multilayer adsorption isotherm models for sorption from aqueous media. Korean J. Chem. Eng., 32(5), 787-799.

Schimmel, D., Fagnani, K.C., Santos, J.B., Barros, M.A. and Silva, E.A. (2010). Adsorption of turquoise blue QG reactive bye commercial activated carbon in batch reactor: kinetic and equilibrium studies. Brazilian Journal of Chemical Engineering, 27 (2), 289-298.

Sen, T. K., Afroze, S. and Ang, H.M., 2011. Equilibrium, kinetics and mechanism of removal of methylene blue from aqueous solution by adsorption onto pine cone biomass of Pinus radiate. Water Air Soil Pollut. 218, 499-515.

Shahmohammadi-Kalalagh, S. and Babazadeh, H. (2014). Isotherms for the sorption of zinc and copper onto kaolinite: comparison of various error functions. Int. J. Environ. Sci. Technol., 11, 111–118.

Tuttuh-Adegun, M. R. and Adegoke, D. G. (2013). New further mathematics project (5^{th} ed.). Bounty press limited, pg 132-133.

Voudrias, E., Fytianos, F. and Bozani, E. (2002). Sorption description isotherms of dyes from aqueous solutions and waste waters with different sorbent materials, Global Nest, The Int.J., 4(1), 75-83.

Wang, X., Jiang, C., Hou, B., Wang, Y., Hao, C. and Wu, J. (2018). Carbon composite lignin-based adsorbents for the adsorption of dyes. Chemosphere, 206, 587-596.

Wong, Y. C., Szeto, Y. S., Cheung, W. H. and McKay, G. (2004) Adsorption of acid dyes on chitosan equilibrium isotherm analyses. Process Biochem, 39(6), 695–704.

Yagub, M.T., Sen, T.K., Afroze, S. and Ang, H.M. (2014). Dye and its removal from aqueous solution by adsorption: A review. Adv. Colloid Interface Sci., 209, 172-184.

Yu, C., Wang, F., Zhang, C., Fu, S. and Lucia, L. A. (2016). The synthesis and absorption dynamics of a lignin-based hydrogel for remediation of cationic dye-contaminated effluent, doi:10.1016/j.reactfunctpolym.2016.07.016.

Supplementary Information

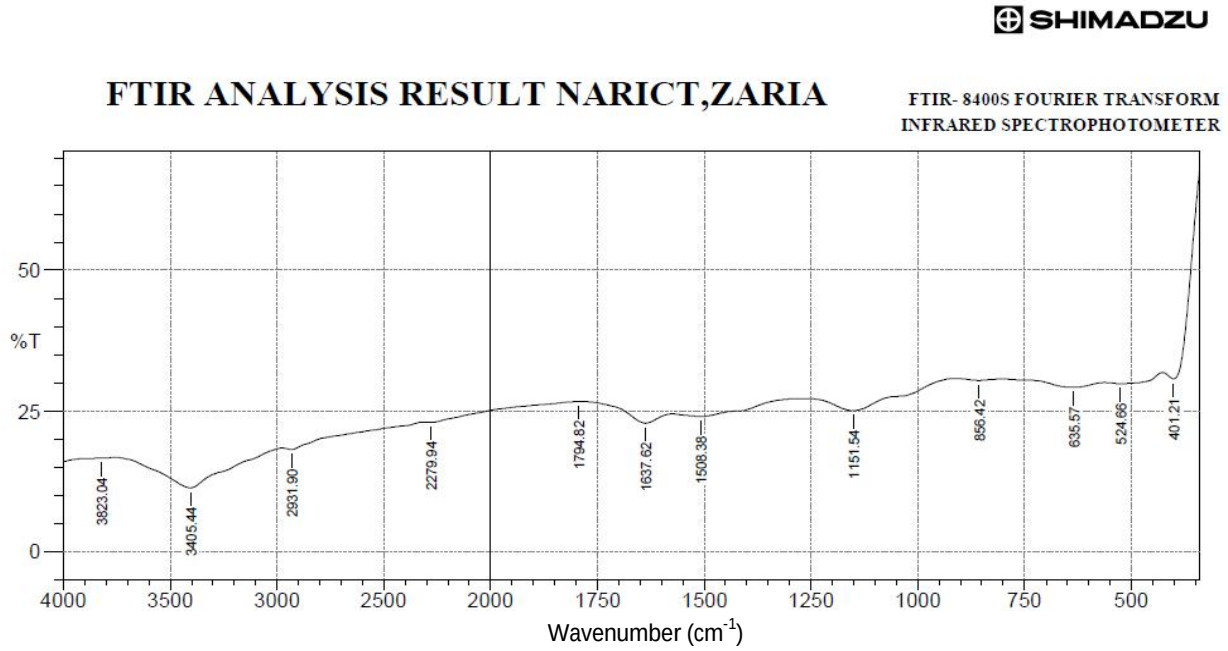

Figure A : FTIR spectrum for AESA

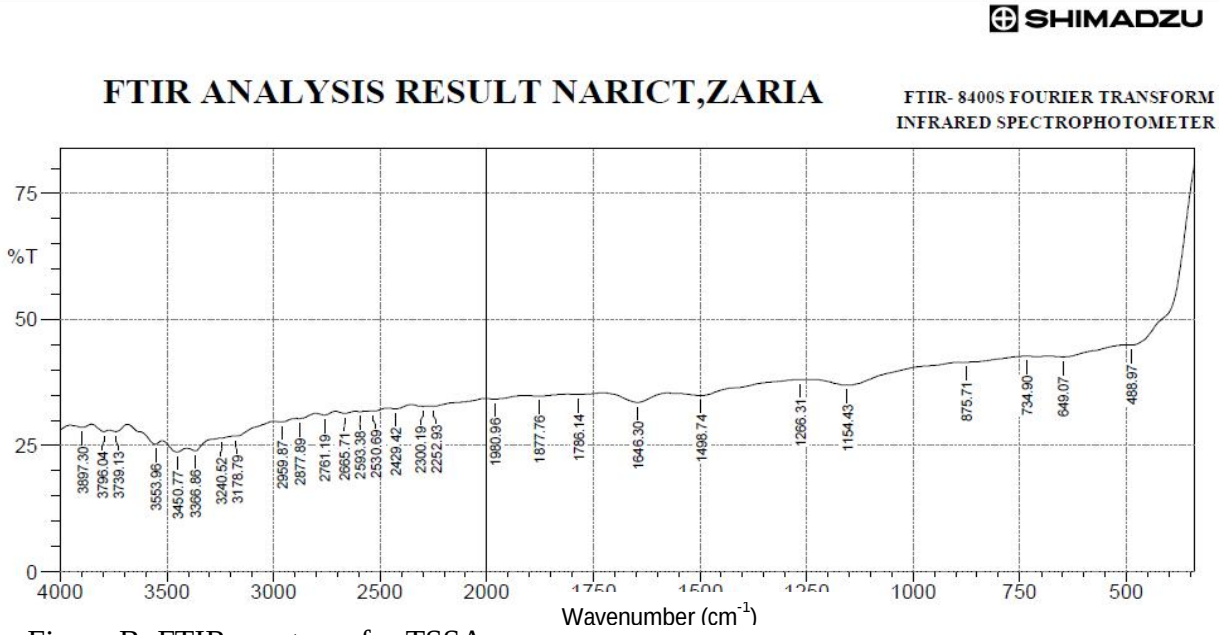

Figure B: FTIR spectrum for TSSA

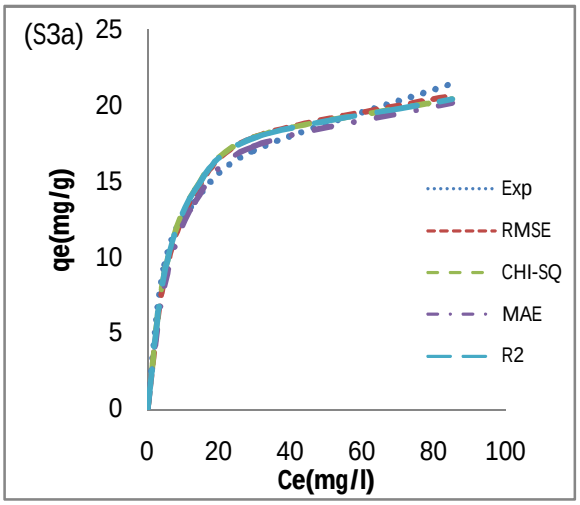
(S3a)
qe(mg/g)
Ce(mg/l)
Exp
RMSE
CHI-SQ
MAE
R2

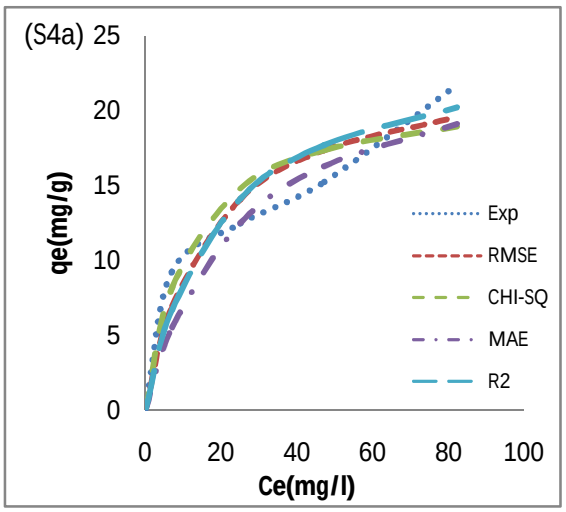
(S4a)
qe(mg/g)
Ce(mg/l)
Exp
RMSE
CHI-SQ
MAE
R2

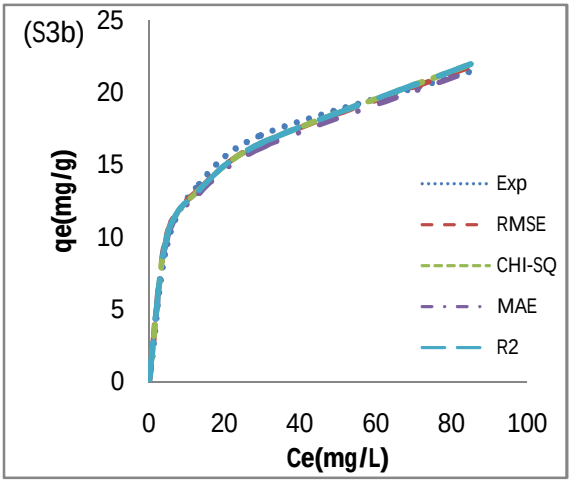
(S3b)
qe(mg/g)
Ce(mg/L)
Exp
RMSE
CHI-SQ
MAE
R2

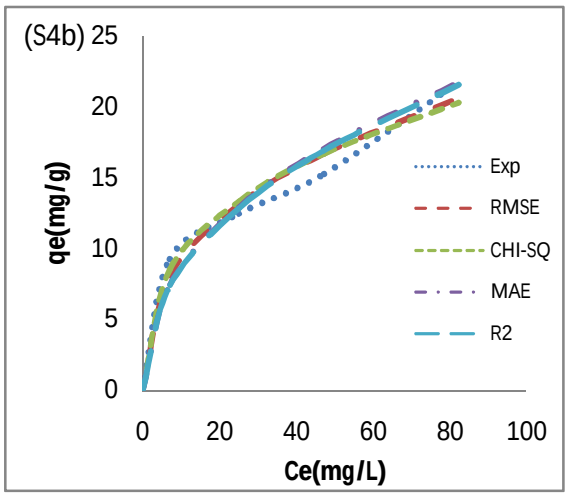
(S4b)
qe(mg/g)
Ce(mg/L)
Exp
RMSE
CHI-SQ
MAE
R2

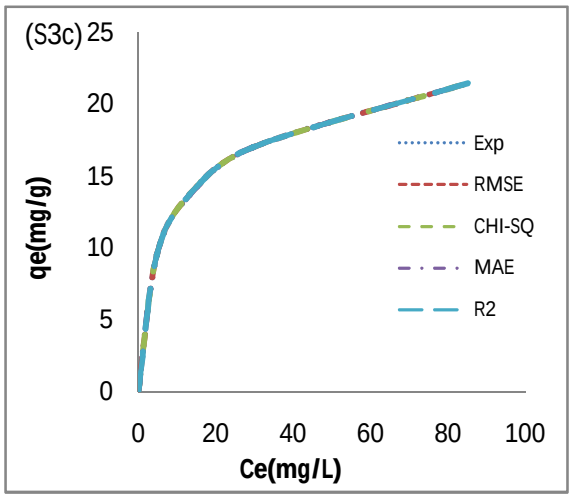
(S3c)
qe(mg/g)
Ce(mg/L)
Exp
RMSE
CHI-SQ
MAE
R2

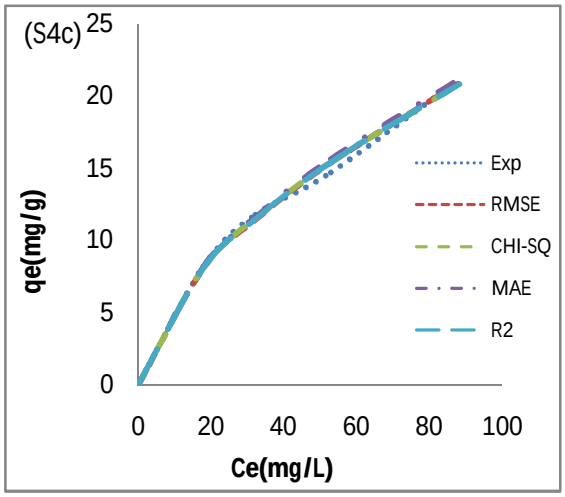
(S4c)
qe(mg/g)
Ce(mg/L)
Exp
RMSE
CHI-SQ
MAE
R2

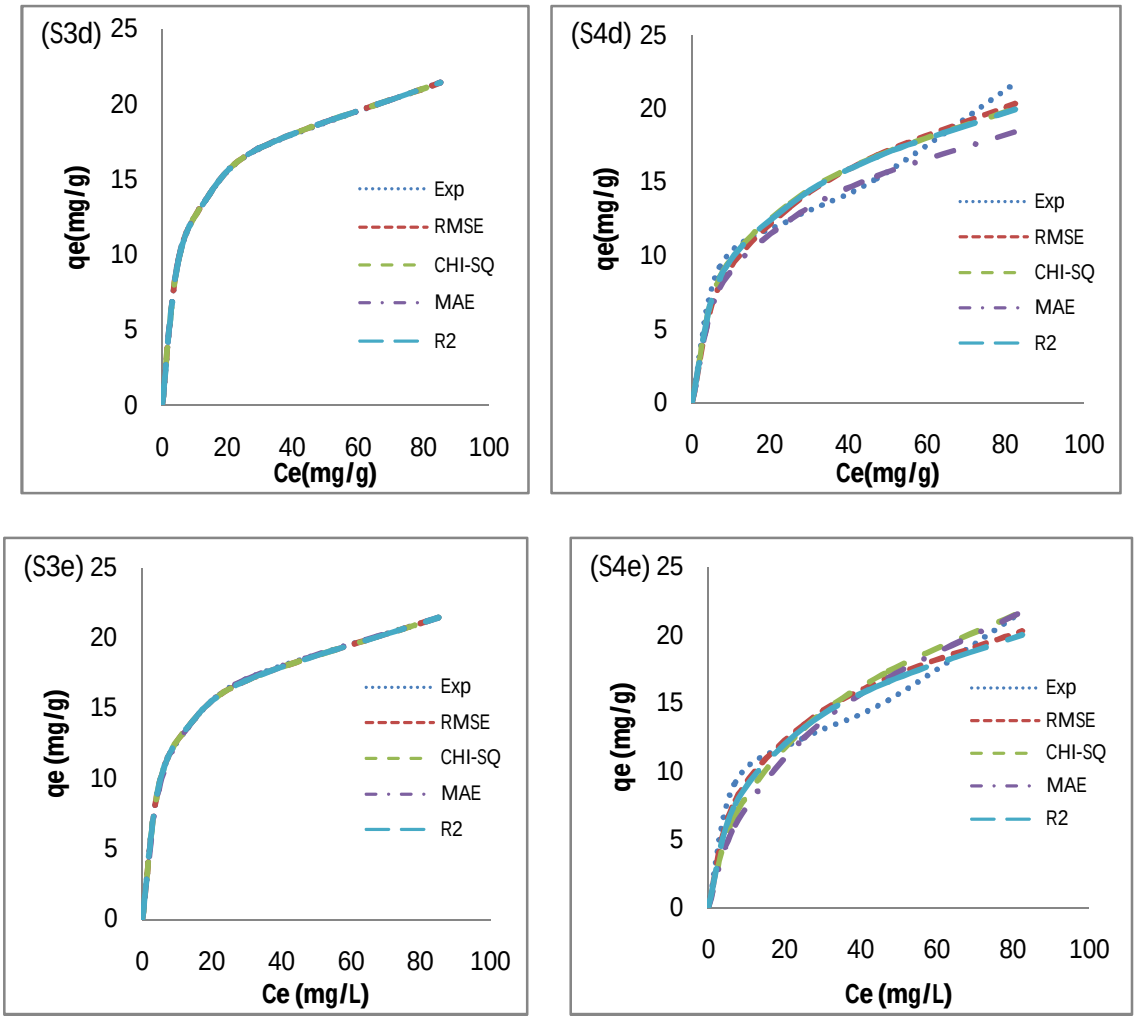

Figures C and D: Fits of isotherm models by minimizing/maximizing error functions for OG onto AESA and TSSA respectively. (a) Langmuir (b) Freundlich (c) R-P (d) Toth (e) Khan

Table A: ANOVA table for AESA and TSSA

	Langmuir	Freundlich	R-P	Toth	Khan
AESA					
P-value	0.99997	1	1	1	1
F-value	0.00342	0.00073	3.03E-07	5.46E-07	3.59E-07
F-critical	2.86608	2.86608	2.86608	2.86608	2.86608
TSSA					
P-value	0.99928	1	0.99956	0.9996	0.99981
F-value	0.01833	0.00017	0.01428	0.01365	0.00945
F-critical	2.86608	2.86608	2.86608	2.86608	2.86608

Table B: Predicted isotherm by minimizing the error distribution using four different error function for AESA

Langmuir (two parameter isotherm)				
AESA	q_m	K_l		OF[a]
R^2	22.1597	0.1421		0.96430
RMSE	22.6083	0.1293		0.7166
Chi-Square	22.1597	0.1429		0.7459
MAE	22.1595	0.1219		0.8637
Freundlich (two parameter isotherm)				
	n	K_f		OF[a]
R^2	3.68676	6.5810		0.98741
RMSE	3.77300	6.7234		0.4336
Chi-Square	3.67276	6.5623		0.4459
MAE	3.73885	6.5472		0.5044
Redlich-Peterson (three parameter isotherm)				
	K_{rp}	a_{rp}	g	OF[a]
R^2	6.73977	0.6499	0.82731	0.99997
RMSE	6.69438	0.6434	0.82804	0.0211
Chi-Square	6.73977	0.6500	0.82730	0.0213
MAE	6.73977	0.6450	0.82741	0.0221
Toth (three parameter isotherm)				
	q_{mT}	b_T	n_T	OF[a]
R^2	37.9379	0.7078	2.77082	0.99998
RMSE	38.1867	0.7233	2.79253	0.0166
Chi-Square	37.9378	0.7081	2.77102	0.0169
MAE	37.9379	0.7082	2.77021	0.0183
Khan (three parameter isotherm)				
	q_{mk}	b_k	a_k	OF[a]
R^2	10.7254	0.5017	0.8097	0.99992
RMSE	10.7996	0.4945	0.8107	0.0342
Chi-Square	10.7261	0.5016	0.8097	0.00039
MAE	11.8872	0.3863	0.8234	0.1001

Table C : Predicted isotherm by minimizing the error distribution using four different error function for TSSA

Langmuir (two parameter isotherm)				
TSSA	q_m	K_l		OF[a]
R^2	24.9680	0.0518		0.83082
RMSE	23.6492	0.0585		1.8438
Chi-Square	21.6620	0.0859		1.9296
MAE	24.9694	0.0398		2.1026
Freundlich (two parameter isotherm)				
	N	K_f		OF[a]
R^2	2.2963	3.1600		0.94989
RMSE	2.6187	3.8329		1.0035
Chi-Square	2.8415	4.3014		1.0396
MAE	2.2876	3.1639		1.1590
Redlich-Peterson (three parameter isotherm)				
	K_{rp}	a_{rp}	g	OF[a]
R^2	9.7661	1.7097	0.7129	0.91809
RMSE	8.4445	1.5791	0.6922	1.1426
Chi-Square	9.7666	1.7057	0.7125	1.2111
MAE	9.7654	1.7134	0.7355	1.7717
Toth (three parameter isotherm)				
	q_{mT}	b_T	n_T	OF[a]
R^2	257.2022	3.2472	6.9256	0.91811
RMSE	257.2210	0.8364	6.1981	1.1483
Chi-Square	257.2022	3.2489	6.9205	1.1852
MAE	257.2015	3.2271	7.0485	1.6051
Khan (three parameter isotherm)				
	q_{mk}	b_k	a_k	OF[a]
R^2	7.3149	0.3481	0.6921	0.9128
RMSE	7.0497	0.4071	0.6924	1.2162
Chi-Square	7.5694	0.2399	0.6357	1.1400
MAE	7.0029	0.2101	0.5907	1.6097

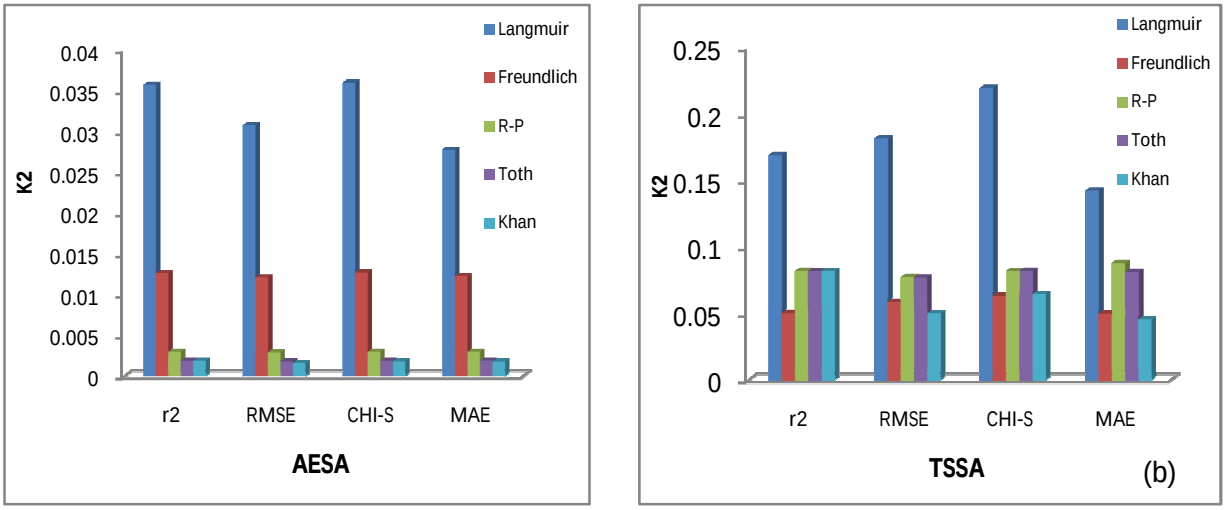

Figure E: Coefficient of non-determination for isotherms of OG adsorbed on (a) AESA and (b) TSSA